Supplementary Materials for

Effects of Fe and Al incorporations on the bridgmanite–postperovskite coexistence domain

Xianlong Wang*, Taku Tsuchiya*, Zhi Zeng

*corresponding author. Email: xlwang@theory.issp.ac.cn (X.W.);

tsuchiya.taku.mg@ehime-u.ac.jp (T.T.)

Materials and Methods

Calculation methods

Calculations are carried out within the framework of the density functional theory (Hohengerg and Kohn, 1964; Khon and Sham, 1965) implemented in the plane-wave self-consistent field (PWSCF) code (Giannozzi et al., 2009) with pseudo-potential method and plane wave basis sets. The kinetic energy cutoff for wave function is set to 50 Ry. To realize a homogenous impurity distribution in PPv, as shown in fig. S1, we use conversion matrix M = (2 0 0, -2 4 0, 0 0 1) to generate the supercells containing 80 atoms, and the irreducible Brillouin zone (IBZ) of the supercells are sampled by a 2×2×2 Monkhorst-Pack grid (Monkhorst and Pack, 1976). The exchange and correlation potential is described by the LSDA+*U* formula, where the *U* values are determined by the internally consistent method (Cococcioni and De Gironcoli, 2005). After atomic structures are fully relaxed, phonon dispersions are calculated by means of the direct lattice dynamic method (Alfè, 2009) with small displacements of 0.01 Å. The local distortions accompanied by the element substitutions are completely included in our simulations, e.g., the Al and LS Fe^{3+} are spontaneously displaced along the *c* direction, when they are substituted at the Mg site of Brg and PPv (Tsuchiya and Tsuchyia, 2008). Furthermore, the quasi-harmonic approximation (QHA) is used to calculate the thermodynamic properties with a 4×4×4 grid sampling of IBZ. The equation of state (EoS) parameters are obtained by fitting the third ordered Birch-Murnaghan EoS (Poirier, 1991). The parameters and pseudo-potentials were widely used in our previous publications (Hsu et al., 2012; Metsue and Tsuchyia, 2012; Tsuchiya and Tsuchyia, 2008; Tsuchiya and Wang, 2013; Wang et al., 2015; Yu et al., 2012). The details about calculations of the Gibbs free energy and determination of the phase transition boundary were presented in our previous work (Metsue and Tsuchyia, 2012) and shown briefly in the supplementary materials. The LDA (GGA) exchange correlation function usually give underestimation (overestimation) of the phase transition pressure (Tsuchiya et al., 2004), moreover, they can output a similar relative phase transition pressure. In current work, the LDA function was used, and all of the discussions rely on the relative PPv phase transition pressure by taking the values of pristine $MgSiO_3$ as a reference.

Supercell selection

As shown in fig. 1A, the lattice constant *a* of the PPv conventional unit cell is notably shorter than that of the lattice constants *b* and *c*, for example, simulated results (Tsuchiya et al., 2004) depending on the LDA exchange and correlation potential show that under 120 GPa, the PPv lattice constant along the *a*, *b*, and *c* directions is 2.462 Å, 8.053 Å, and 6.108 Å, respectively. Therefore, if the matrix of M = (2 0 0, 0 2 0, 0 0 2) is used for constructing the PPv supercell, the homogeneous impurity distributions in the supercell with the lattice constants of $a' = 2a$, $b' = 2b$, and $c' = 2c$ cannot be realized. In the current

work, for generating homogeneous impurity distributions (Tsuchiya ad Tsuchyia, 2008), we use the matrix of M = (2 0 0, -2 4 0, 0 0 1) to generate a PPv supercell containing 80 atoms and giving rise to an impurity concentration of 6.25 mol%, which are shown in fig. 1B. In our previous work for the determination of two-phase coexistence domain of $Al^{3+}Al^{3+}O_3$-bearing case (Tsuchiya, 2008), we confirmed that the results using the 80 atom supercell were almost same as those of the 160 atom supercell, indicating that 80 atom supercell employed in this study is enough.

Fe and Al configurations in PPv

The Fe and Al configurations in PPv with 12.5 mol% Fe and 12.5 mol% Al had been reported in previous works (Hsu et al., 2012; Yu etg al., 2012). Within the pressure range of the lowest mantle, Fe substituted at the Mg site and the Si site has a high spin (HS) state and a low spin (LS) state, respectively. In the presence of Al^{3+}, HS Fe^{3+} tends to stay at the Mg site with Al^{3+} occupying the Si site. Using the generated supercell containing 80 atoms as mentioned above, the impurity configurations of 6.25 mol% Fe and 6.25 mol% Al-bearing PPv are clarified. Around the pressure range of core-mantle boundary, Fe^{2+} substituted at the Mg site has the HS sate resulting in a configuration of $(Mg,Fe^{2+}_{HS})SiO_3$ (Yu et al., 2012), similar to Brg (Yu et al., 2012). The calculated relative enthalpies of PPv incorporated with 6.25 mol% $Fe^{3+}Fe^{3+}O_3$ and 6.25 mol% $Fe^{3+}Al^{3+}O_3$ are shown in fig. S2. For the $Fe^{3+}Fe^{3+}O_3$-bearing case, $(Mg,Fe^{3+}_{HS})(Si,Fe^{3+}_{HS})O_3$ is the most stable in the lower pressure range, moreover, a spin transition (from HS to LS state) occurs in the Si site under a pressure of ~25 GPa corresponding to the configuration transition: from $(Mg,Fe^{3+}_{HS})(Si,Fe^{3+}_{HS})O_3$ to $(Mg,Fe^{3+}_{HS})(Si,Fe^{3+}_{LS})O_3$. Up to a pressure of 180 GPa, $(Mg,Fe^{3+}_{HS})(Si,Fe^{3+}_{LS})O_3$ is the most stable configuration, and $(Mg,Fe^{3+}_{LS})(Si,Fe^{3+}_{LS})O_3$ has a larger enthalpy than that of $(Mg,Fe^{3+}_{HS})(Si,Fe^{3+}_{LS})O_3$. Note that, the $(Mg,Fe^{3+}_{LS})(Si,Fe^{3+}_{HS})O_3$ is a stable configuration only under pressures ranging from 0 GPa to 10 GPa, and it transfers to $(Mg,Fe^{3+}_{HS})(Si,Fe^{3+}_{LS})O_3$ spontaneously at a pressure of 20 GPa. In the high-*P* range, above 50 GPa, our results agree well with previous reports for the $Fe^{3+}Fe^{3+}O_3$-bearing case (Tsuchiya and Wang, 2013). Similar to the results of $Fe^{3+}Fe^{3+}O_3$-bearing Brg, where Fe^{3+} in the Si site undergoes a spin transition at a pressure of ~55 GPa, Fe^{3+} substituted at the Si site of PPv will also experience a spin transition at a pressure of ~23 GPa. Whereas, there is no spin transition of Fe^{3+} at the PPv Si site in the previous report (Nakajima et al., 2012) based on LSDA+*U* method. For PPv incorporation with 6.25 mol% $Fe^{3+}Al^{3+}O_3$, the most stable configuration is $(Mg,Fe^{3+}_{HS})(Si,Al^{3+})O_3$ up to a pressure of 180 GPa. In the high-*P* range, from 50 GPa to 180 GPa, PPv with 6.25 mol% Fe and 6.25 mol% Al has the same chemical configuration as that of the 12.5 mol% Fe and 12.5 mol% Al-bearing cases, indicating that when incorporated with ~12.5 mol% Fe and Al, the ground sate of Fe and Al-bearing PPv should be $(Mg,Fe^{2+}_{HS})SiO_3$, $(Mg,Fe^{3+}_{HS})(Si,Fe^{3+}_{LS})O_3$, $(Mg,Fe^{3+}_{HS})(Si,Al^{3+})O_3$, $(Mg,Al^{3+})(Si,Al^{3+})O_3$.

Phonon dispersions and thermodynamic properties

A negative frequency is not found in the simulated phonon dispersions for all Fe/Al-bearing cases beyond 70 GPa, for example, phonon dispersions of (Mg,Fe^{3+}_{HS})(Si,Al^{3+})O_3 PPv at 120 GPa (fig. S3). The results indicate that PPv incorporated with a small amount of Fe and Al (~6.25 mol%) is kinetically stable. From the vibrational density of state of (Mg,Fe^{3+}_{HS})(Si,Al^{3+})O_3 PPv at 120 GPa, we can find that Fe^{3+} and Al^{3+} mainly contributes to the low and middle frequencies, respectively, since the ionic weight of Fe is larger than that of Al, Si, and Mg. The calculated thermodynamic parameters of (Mg,Al^{3+})(Si,Al^{3+})O_3 Brg, (Mg,Fe^{3+}_{HS})(Si,Fe^{3+}_{LS})O_3 PPv, (Mg,Fe^{3+}_{HS})(Si,Al^{3+})O_3 PPv, and (Mg,Al^{3+})(Si,Al^{3+})O_3 PPv at 100 GPa are presented in table S1, indicating that similar to our previous findings on Fe^{2+}-bearing Brg (Metsue and Tsuchyia, 2012), $Fe^{3+}Fe^{3+}$-bearing Brg (Tsuchiya and Wang , 2013), $Fe^{3+}Al^{3+}$-bearing Brg (*2*), and Fe^{2+}-bearing PPv (Alfè, 2009), 6.25 mol% Fe and Al incorporations have insignificant effects on the thermodynamic properties except for the Grüneisen parameter.

Calculation of the Gibbs free energy and determination of the PPv phase transition boundary

For Fe and Al-bearing Brg and PPv, the total Gibbs free energy $G(P, T, x)$ at the Fe/Al concentration of x is given by the general expression for a binary system, as shown:

$$G_\alpha(P,T,x) = xG_\alpha^{end-member} + (1-x)G_\alpha^{pristine} - TS_{conf}, \quad (1)$$

In eq. 1, α means Brg or PPv, $G^{pristine}$ and $G^{end\text{-}member}$ is the Gibbs free energy of pristine $MgSiO_3$ and the end member of Fe/Al-bearing $MgSiO_3$, for example, the end members of Fe^{2+}- and $Fe^{3+}Al^{3+}$-bearing $MgSiO_3$ are $FeSiO_3$ and $FeAlO_3$, respectively. S_{conf} is the configurational contributions to entropy. Following, the Gibbs energy of $MgSiO_3$ incorporated with a small amount of $Fe^{3+}Al^{3+}O_3$ is calculated by

$$G_\alpha(P,T,x) = x\{\frac{[E_\alpha^{0.0625FeAl-bearing}(P,T) + PV_\alpha^{0.0625FeAl-bearing}(P,V) + F_{vib-\alpha}^{0.0625FeAl-bearing}] - 0.9375G_\alpha^{pristine}(P,T)}{0.0625}$$

$$-TS_{mag}\} + (1-x)G_\alpha^{pristine}(P,T) - TS_{conf}, \quad (2)$$

where, $E^{0.0625FeAl\text{-}bearing}$ means the static energy of 6.25 mol% $Fe^{3+}Al^{3+}O_3$-bearing $MgSiO_3$. The vibrational contributions to free energy ($F_{vib}^{0.0625FeAl-bearing}$) is calculated by equation (3) using the quasi-harmonic approximation (QHA) based on the simulated phonon dispersions,

$$F_{vib}^{0.0625-bearing}(V,T) = \frac{1}{2}\sum_{q,j} h\omega_j(q,V) + k_BT\sum_{q,j}\ln[1-\exp(-h\omega_j(q,V)/k_BT)], \quad (3)$$

where, the first term is the zero point vibrational energy, and vibrational contributions are shown in the second term. ω_j is the phonon frequency. S_{mag} and S_{conf} are the magnetic and configurational contributions to entropy, and the magnetic contributions to entropy is derived from the following equation:

$$S_{mag} = -k_B X_{Fe} \ln[m(2S+1)]. \quad (4)$$

In the equation, k_B is the Boltzmann constant. X_{Fe}, m, and S represent the concentration of Fe, the total spin quantum number, and the electronic configuration degeneracy, respectively. Taking the high spin state (HS) $Fe^{2+}SiO_3$-bearing $MgSiO_3$ for instance, X_{Fe}, m, and S are equal to 0.0625, 1, and 2, respectively. For ideal mixing, the configurational contribution, S_{conf}, is given by

$$S_{conf} = -k_B[X_{Fe} \ln(X_{Fe}) + (1 - X_{Fe}) \ln(1 - X_{Fe})]. \quad (5)$$

Note that previous theoretical studies prove that for the incorporation of the $FeAlO_3$ component to Brg and PPv, Fe and Al atoms tend to be paired in the stable configuration, where Fe and Al are substituted at the Mg site and neighboring Si site, respectively (Hsu et al., 2012; Wang et al., 2015). Our previous simulations of the Al-bearing system (Tsuchiya and Tsuchiya, 2008), considering ~200 different randomly chosen cation configurations with various $Al^{3+}Al^{3+}O_3$ concentration from 0 to 1 for a full treatment of non-ideality, showed that ~6.25 mol% $Al^{3+}Al^{3+}O_3$ incorporation decreases the PPv phase transition pressure a bit at 2500 K with a narrow TPC domain. The present phase diagram of the Al-bearing system is in excellent agreement with this previous result, indicating that ideal mixing entropy applied in this work is sufficient.

As a function of $Fe^{2+}SiO_3$ and $Fe^{3+}Fe^{3+}O_3$ concentration, the calculated Gibbs free energy of Brg and PPv at high-P and high-T conditions is shown in fig. S5. We can find that at 2500 K and 114 GPa, the Gibbs free energy of PPv is larger than that of Brg within the $Fe^{2+}SiO_3$ concentration of 16 mol% indicating that Brg is a stable phase in the current conditions. At 120 GPa, the two curves cross over, and the phase transition occurs. The Gibbs free energy of PPv is smaller than that of Brg at 126 GPa, indicating the completion of the phase transition.

By calculating the common tangent of two crossed curves, as shown in fig. S5, the Fe concentrations in Brg and PPv can be determined, and they will decrease with increasing pressure at temperature T'. We then search the two pressures where the concentrations of Fe in Brg and PPv are equal to the concentration of x', which give the two phases coexisting domain at T' and x'. By changing the values of T and x, we can get the pressure range of two-phase coexisting at certain temperatures and certain impurity concentrations.

The two-phase coexistence domain of 6.25 mol% $Fe^{2+}SiO_3$-bearing Brg was reported in our previous work based on the same method (Metsue and Tsuchyia, 2012). However, an unreasonable temperature dependence of the coexistence domain (i.e., the two-phase width decreases with increasing temperature, see Fig. 1A) was seen. After reanalyzing this system in the current work using high-resolution free energy data, such temperature dependence disappears. We also perform calculations of $Al^{3+}Al^{3+}O_3$-bearing Brg to confirm the previous investigation (Caracas and Cohen, 2008).

Crystallographic origin of the difference in the two-phase loop between $Fe^{2+}SiO_3$- and $Fe^{3+}Fe^{3+}O_3$-bearing $MgSiO_3$

The different PPv phase transition behaviors between Fe^{2+}- and Fe^{3+}-bearing $MgSiO_3$ can be understood by the following: Since the key process of the PPv phase transition is octahedral tilting (Tsuchiya et al., 2004), for the same element substitution (such as Fe^{2+} and Fe^{3+}), the size of the ion substituted at the Mg site will play an important role for determining the phase transition pressure, and the octahedral tilting is easier when a smaller ion occupies the Mg site resulting in a lower phase transition pressure. The ionic radius of HS Fe^{3+} is 78.5 pm notably smaller than that of HS Fe^{2+} (92 pm), therefore, the PPv phase transition pressure of $(Mg,Fe^{3+}_{HS})(Si,Fe^{3+}_{LS})O_3$ (-4.3 GPa at 0 K) is lower than $(Mg,Fe^{2+}_{HS})SiO_3$ (-2.5 GPa at 0 K) (table S2). The deviation of the PPv phase transition pressure between $(Mg,Fe^{3+}_{HS})(Si,Fe^{3+}_{LS})O_3$ and pristine $MgSiO_3$ is larger than that of $(Mg,Fe^{2+}_{HS})SiO_3$, giving rise to a bigger slope difference of the free energy curves between Brg and PPv for $(Mg,Fe^{3+}_{HS})(Si,Fe^{3+}_{LS})O_3$, as shown in fig. S5. Therefore, the discrepancy of the Fe concentrations between Brg and PPv determined by the common tangent in the case of $(Mg,Fe^{3+}_{HS})(Si,Fe^{3+}_{LS})O_3$ (fig. S5E) is larger than that of $(Mg,Fe^{2+}_{HS})SiO_3$ (fig. S5B) resulting in a broader two-phase coexistence domain of $(Mg,Fe^{3+}_{HS})(Si,Fe^{3+}_{LS})O_3$.

Computational uncertainties

In the first principles simulations, the uncertainties are yielded mainly from approximations and calculation conditions, such as pseudo-potentials, exchange-correlation functional (LDA or GGA), kinetic energy cutoff, and k-point sampling. For example, the phase transition pressures calculated based on LDA are generally ~10 GPa lower than those of GGA. However, in this work, we focus on the relative differences between Brg and PPv. Therefore, the uncertainties caused by these factors would be mostly cancelled. Furthermore, to reduce the numerical uncertainties, a strict convergence threshold of 1.0×10^{-9} Ry (1.0×10^{-5} Ry/Bohr) is set to calculate total energies (forces acting on atoms) for all the calculations. As shown in the fig. S4 and our previous results (Metsue and Tsuchyia, 2012; Tsuchiya and Wang, 2013; Wang et al., 2015), predicted *P-V-T* equation of states of Fe- and Al-bearing Brg and PPv based on the framework and parameters used in this work agree well with experimental

observations under the pressure ranging from 0 GPa to 140 GPa. The results indicate that the uncertainties of volume estimation are small, which is typically less than 0.05 cm^3/mol.

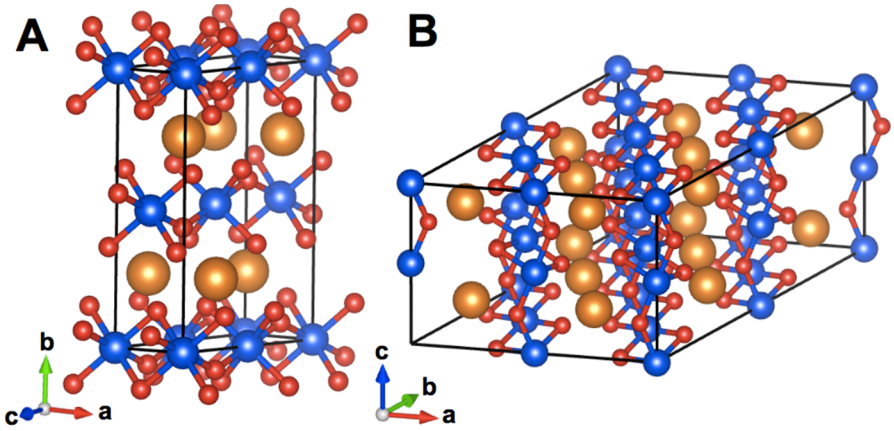

Fig. S1.

Crystal structure of PPv. **(A)** Conventional unit cell of PPv. **(B)** PPv supercell generated using conversion matrix M = (2 0 0, -2 4 0, 0 0 1).

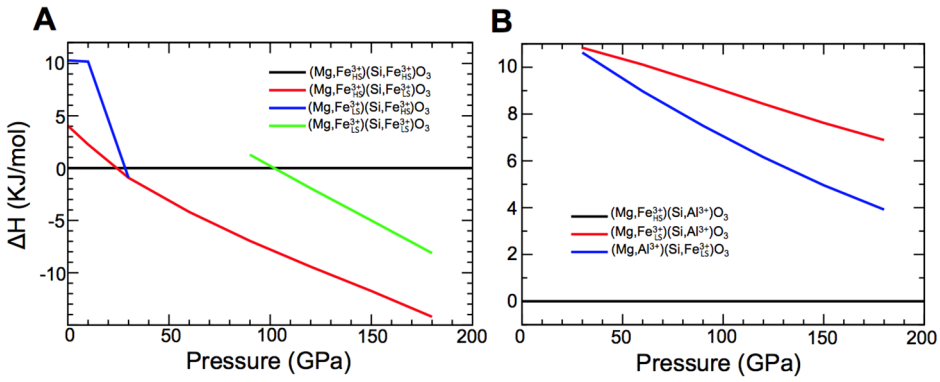

Fig. S2.

Relative enthalpies of $Fe^{3+}Al^{3+}$-bearing PPv. **(A)** Relative enthalpies of 6.25 mol% $Fe^{3+}Fe^{3+}O_3$-bearing PPv, the enthalpy of (Mg,Fe^{3+}_{HS})(Si,Fe^{3+}_{HS})O_3 is set to zero. **(B)** Relative enthalpies of PPv with 6.25 mol% Fe^{3+} and 6.25 mol% Al^{3+} incorporations, the enthalpy of (Mg,Fe^{3+}_{HS})(Si,Al^{3+})O_3 is set to zero.

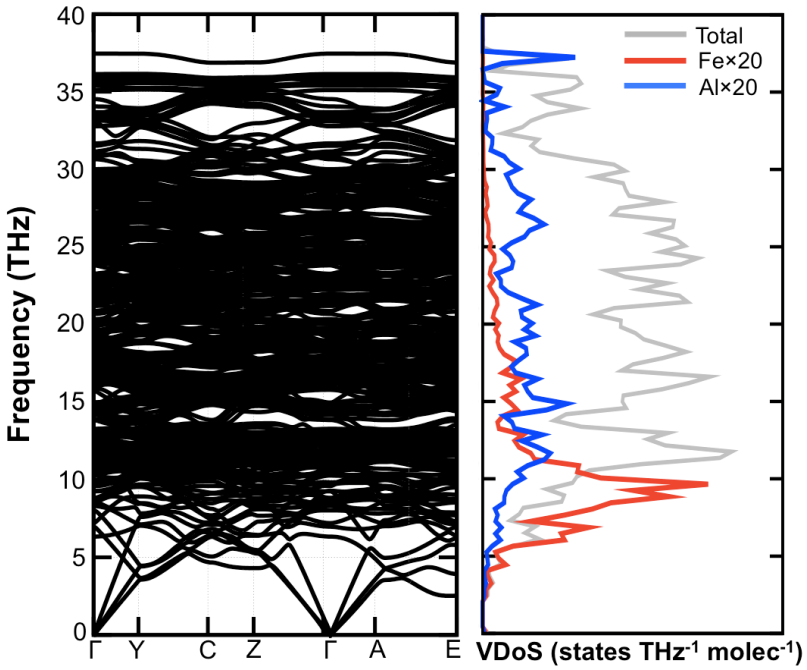

Fig. S3.

Phonon dispersions and vibrational density of states (VDoS) of (Mg,Fe^{3+}_{HS})(Si,Al^{3+})O_3 at 120 GPa. Grey, red, and blue lines represent the total VDoS and partial VDoS of both Fe^{3+} and Al^{3+}, respectively. The supercells containing 80 atoms have a total of 240 phonon modes. The concentration of $Fe^{3+}Al^{3+}O_3$ is 6.25 mol%.

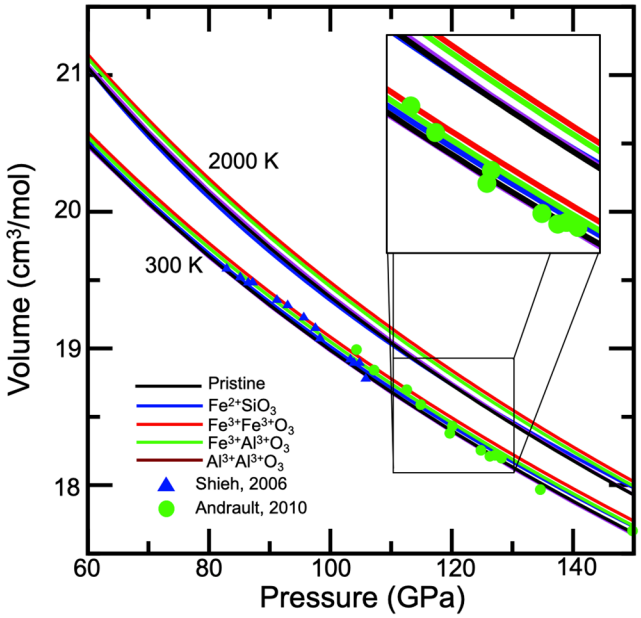

Fig. S4.

Volume compression curves of PPv at 300 K and 2000 K isotherms. Black, blue, red, green, and purple lines show the compression curves of pure $MgSiO_3$, $(Mg,Fe^{2+}_{HS})SiO_3$, $(Mg,Fe^{3+}_{HS})(Si,Fe^{3+}_{LS})O_3$, $(Mg,Fe^{3+}_{HS})(Si,Al^{3+})O_3$, $(Mg,Al^{3+})(Si,Al^{3+})O_3$, respectively, The Fe/Al concentrations are set to 6.25 mol%. Experimental results of PPv with 9 mol% $Fe^{2+}SiO_3$ (Shieh et al., 2006) and 15 mol% $Fe^{3+}Al^{3+}O_3$ (Andrault et al., 2010) are shown in blue triangles and green dots, respectively. Volumes between 115 GPa and 125 GPa are zoomed in in the inset.

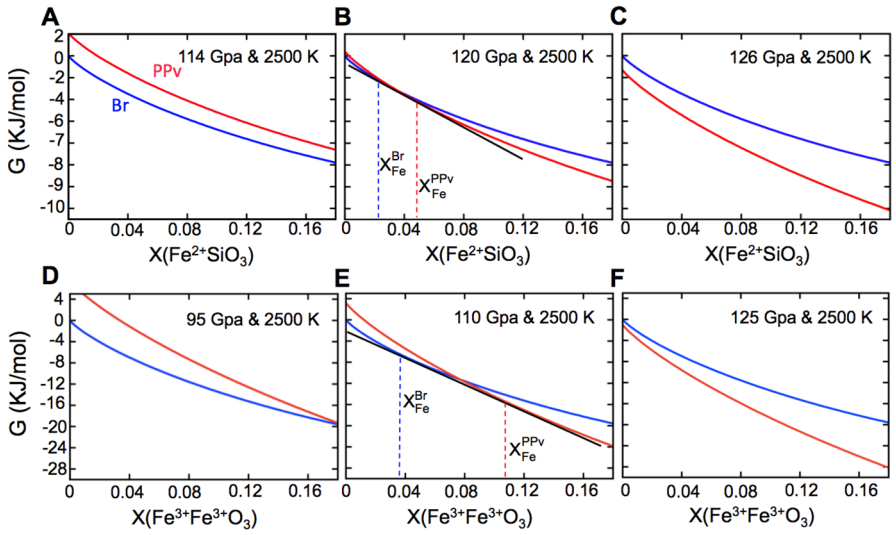

Fig. S5.

The Gibbs free energy variations at 2500 K. (A) $Fe^{2+}SiO_3$-bearing case at 114 GPa. **(B)** $Fe^{2+}SiO_3$-bearing case at 120 GPa. **(C)** $Fe^{2+}SiO_3$-bearing case at 126 GPa. **(D)** $Fe^{3+}Fe^{3+}O_3$-bearing case at 95 GPa. **(E)** $Fe^{3+}Fe^{3+}O_3$-bearing case at 110 GPa. **(F)** $Fe^{3+}Fe^{3+}O_3$-bearing case at 125 GPa. With taking the value of pure $MgSiO_3$ Brg as a reference, the Gibbs free energy variations of Brg (blue) and PPv (red) solid solutions are shown. The common tangent of the Brg and PPv curves is shown by the black solid line.

2. Supplementary Tables

Table S1.

Thermodynamic parameters at 100 GPa. The thermal expansivity, isothermal bulk modulus, isobaric heat capacity, and Grüneisen parameter of 6.25 mol% $Al^{3+}Al^{3+}O_3$-bearing Brg, 6.25 mol% $Fe^{3+}Fe^{3+}O_3$-bearing PPv, 6.25 mol% $Fe^{3+}Al^{3+}O_3$-bearing PPv, and 6.25 mol% $Al^{3+}Al^{3+}O_3$-bearing PPv. The values of pristine phases, $MgSiO_3$-Brg and $MgSiO_3$-PPv, are shown in brackets.

	$Al^{3+}Al^{3+}O_3$-Brg		$Fe^{3+}Fe^{3+}O_3$-PPv		$Fe^{3+}Al^{3+}O_3$-PPv		$Al^{3+}Al^{3+}O_3$-PPv	
	300 K	2000 K	300 K	2000 K	300 K	2000 K	300 K	2000 K
α ($10^{-5}K^{-1}$)	0.64	1.39	0.64	1.39	0.65	1.40	0.67	1.43
	(0.59)	(1.32)	(0.60)	(1.35)				
B_T (GPa)	598.30	556.96	602.22	560.66	600.11	558.60	599.19	555.00
	(601.54)	(564.23)	(599.63)	(558.29)				
Cp ($Jmol^{-1}K^{-1}$)	61.04	126.40	61.00	126.43	60.67	126.47	60.34	126.62
	(60.88)	(125.98)	(59.74)	(126.09)				
γ	1.22	1.25	1.22	1.24	1.23	1.26	1.25	1.26
	(1.13)	(1.20)	(1.15)	(1.20)				

Table S2.

Shifts of the PPv transition pressure. Shifts of the PPv transition pressure from pure $MgSiO_3$ at 0 K and 2500 K in multi-component systems with 6.25 mol% $Fe^{2+}SiO_3$, $Al^{3+}Al^{3+}O_3$, $Fe^{3+}Fe^{3+}O_3$, and $Fe^{3+}Al^{3+}O_3$. The calculated transition pressures for pure $MgSiO_3$ are 95.4 and 121.4 GPa at 0 and 2500 K, respectively. The calculated shift of the PPv transition pressure of 6.25 mol% Fe^{2+}-bearing $MgSiO_3$ at 2500 K is given in bracket (Caracas and Cohen, 2008). The unit of pressure is GPa.

T (K)	$Fe^{2+}SiO_3$	$Al^{3+}Al^{3+}O_3$	$MgSiO_3$	$Fe^{3+}Fe^{3+}O_3$	$Fe^{3+}Al^{3+}O_3$
0	-2.5	3.4	0.0	-4.3	0.5
2500	-2.8 ~ -2.0 (-12.8 ~ -9.0)	-5.7 ~ -3.4	0.0	-15.3 ~ -6.5	-24.6 ~ -7.8

References

Alfè, D., 2009. PHON: A program to calculate phonons using the small displacement method. Comput. Phys. Commun. 180, 2622–2633.

Andrault, D., Muñoz, M., Bolfan-Casanova, N., Guignot, N., Perrillat, J.-P., Aquilanti, G. Pascarelli, S.D., 2010. Experimental evidence forr perovskite and post-perovskite coexistence throughout the whole D'' region. Earth Planet Sci. Lett. 293, 90-96.

Caracas, R., Cohen, R.E., 2008. Ferrous iron ion post-perovskite from the first-principles calculations. Phys. Earth Planet Inter. 168, 147-152.

Cococcioni, M., de Gironcoli, S., 2005. Linear response approach to the calculation of the effective interaction parameters in the LDA+U method. Phys. Rev. B 71, 35105.

Giannozzi, P., et al., 2009. QUANTUM ESPRESSO: a modular and open-source software project for quantum simulations of materials. J. Phys. Condens. Matter 21, 395502

Hohengerg, P., Kohn, W., 1964. Inhomogeneous electron gas, Phys. Rev. 136, B864–B871.

Hsu, H., Yu, Y. G., Wentzcovitch, R. M., 2012. Spin crossover of iron in aluminous MgSiO3 perovskite and post-perovskite. Earth Planet. Sci. Lett. 359-360, 34–39.

Kohn, W., Sham, L. J., 1965. Quantum density oscillations in an inhomogeneous electron gas. Phys. Rev. 123, A1697–A1705.

Metsue, A., Tsuchiya, T., 2011. Lattice dynamics and thermodynamic properties of $(Mg,Fe^{2+})SiO_3$ post-perovskite. J. Geophys. Res. 116, B08207.

Monkhorst, H. J., Pack, J. D., 1976. Special points for Brillouin-zone integrations. Phys. Rev. B 13, 5188–5192.

Nakajima, Y., Frost, D.J., Rubie, D.C., 2012 .Ferrous iron partitionong between magnesium silicate perovskite and ferropericlase and the composition of perovskite in the Earth's lower mantle. J. Geophys. Res. 117, BO8201.

Poirier, J.-P., 1991. Introduction to the Physics of the Earth's Interior. Cambridge

University Press.

Shieh, S.R., Duffy, T.S., Kubo, A., Shen, G.Y., Prakapenka, V.B., Sara, N., Hirose, K., Ohishi, Y., 2006. Equation of state of the post-perovskite phase synthetized from a natural (Mg, Fe) SiO_3 orthopyroxene. Proc. Natl. Acad; sci. U. S. A. 103, 3039-3043.

Tsuchiya, J., Tsuchiya, T., 2008. Post-perovskite phase equilibria in the $MgSiO_3$-Al_20_3. Proc. Natl. Acad. Sci. U. S. A. 105, 19160-19164.

Tsuchiya, T., Wang, X., 2013. Ab initio investigation on the high-temperature thermodynamic properties of Fe^{3+}-bearing $MgSiO_3$ perovskite. J. Geophys. Res.: Solid Earth 118, 83-91.

Tsuchyia, T., Tsuchiya, J., Umemoto, K., Wentzcovitch, R.M., 2004. Phase transition in $MgSiO_3$ perovskite in the earth's lower mantle. Earth Planet Sci. Lett. 224, 241-248. Wang, X.L., Tsuchiya, T., Hase, A., 2015. Computational support for a pyrolitic lower mantle containing ferric iron. Nat. Geosci. 8, 556-559.

Yu, Y., Hsu, H., Cococcioni, M., Wentzcovitch, R.M., 2012. Spin states and hyperfine interactions of iron incorporated in $MgSiO_3$ post-perovskite. Earth Planet Sci. Lett. 331, 1-7.